Towards a Stable Numerical Evolution of Strongly Gravitating Systems in General Relativity: The Conformal Treatments

Miguel Alcubierre(1), Bernd Brügmann(1), Thomas Dramlitsch(1), José A. Font(2), Philippos Papadopoulos(3), Edward Seidel(1,4), Nikolaos Stergioulas(1,5) and Ryoji Takahashi(1)

(1) *Max-Planck-Institut für Gravitationsphysik, Am Mühlenberg 1, D-14476 Golm, Germany*
(2) *Max-Planck-Institut für Astrophysik, Karl-Schwarzschild-Str. 1, D-85740 Garching, Germany*
(3) *School of Computer Science and Maths, University of Portsmouth, Portsmouth PO1 2EG, United Kingdom*
(4) *National Center for Supercomputing Applications, Beckman Institute, 405 N. Mathews Ave., Urbana, IL 61801*
(5) *Department of Physics, Aristotle University of Thessaloniki, Thessaloniki 54006, Greece*

(March 20, 2000; AEI-2000-021)

We study the stability of three-dimensional numerical evolutions of the Einstein equations, comparing the standard ADM formulation to variations on a family of formulations that separate out the conformal and traceless parts of the system. We develop an implementation of the conformal-traceless (CT) approach that has improved stability properties in evolving weak *and* strong gravitational fields, and for both vacuum *and* spacetimes with active coupling to matter sources. Cases studied include weak and strong gravitational wave packets, black holes, boson stars and neutron stars. We show under what conditions the CT approach gives better results in 3D numerical evolutions compared to the ADM formulation. In particular, we show that our implementation of the CT approach gives more long term stable evolutions than ADM in all the cases studied, but is less accurate in the short term for the range of resolutions used in our 3D simulations.

04.25.Dm, 04.30.Db, 97.60.Lf, 95.30.Sf

I. INTRODUCTION

Three dimensional (3D) numerical relativity is an important technique for exploring the strong field dynamics in realistic astrophysical phenomena involving black holes and neutron stars. It is expected to play a role in analyzing gravitational waveforms to be observed soon, one expects, with the new generation of gravitational wave detectors going online worldwide in the next few years [1,2]. However, progress in 3D numerical relativity, which has traditionally been based on the Arnowitt-Deser-Misner (ADM) [3] system of evolution equations, has been slow. This is not only because of the immense computational difficulties that 3D simulations represent, but to a large extent it is due to severe instabilities often encountered during such simulations. Presently there is no complete understanding of the causes of these instabilities in numerical evolutions of the ADM equations. This has prompted much recent effort in developing alternative formulations of the 3+1 Einstein equations.

In this and a companion paper [4] we focus on an alternative approach based on a conformal decomposition of the metric and the trace-free components of the extrinsic curvature. The conformal-tracefree (CT) approach was first devised by Nakamura in the 1980's in 3D calculations [5,6], and then modified and applied to work on gravitational waves [7], and on neutron stars [8,9]. This approach was not taken up by others in the community until a recent paper by Baumgarte and Shapiro [10], where a similar formulation was compared with the standard ADM approach and shown to be superior, in terms of both accuracy and stability, on tests involving weak gravitational waves, with geodesic and harmonic slicing. In a followup paper, Baumgarte, Hughes, and Shapiro [11] applied the same formulation to systems with given (analytically prescribed) matter sources, and found similar stability properties. More recently fully hydrodynamical simulations employing the CT approach have been reported in [12–14] in the context of collapse of rapidly-rotating (isolated) neutron stars and coalescence and merge of binary neutron stars.

In the companion paper [4] we perform an analytic investigation of the stability properties of the ADM and the CT evolution equations. Using a linearized plane wave analysis, we identify features of the equations that we believe are responsible for the difference in their stability properties.

In this paper we report the results of simulations of weak and strong gravitational wave packets, black holes, boson stars and neutron stars in various slicing conditions, including maximal slicing and a family of algebraic slicings, and compare the results obtained by the ADM and CT equations in different implementations. We begin with a brief presentation of the relevant equations in Sec. II. We then discuss the results of our numerical simulations in section III. We consider vacuum spacetimes in section III A, and matter spacetimes in section III B. In section III A 1, we describe the various implementations of the CT equations using gravitational wave spacetimes as an example. We identify two particular implementations, which we call AFA and AF2, that give the best performance in long term evolutions. The essence of these implementations, is to "actively force" (AF, see below) the trace of the conformally rescaled extrinsic curvature (AFA), and for maximal slicing also the trace of the extrinsic curvature (AF2), to zero in each step of the numerical evolution. In the sections that follow, we focus on comparing the AFA and AF2 implementations to the results of the ADM equations for evolutions of strong field systems including black holes, boson stars and neutron stars. We demonstrate that for this wide range of systems, these two implementations of the CT equations always lead to more stable long term evolutions. However, we also find that for a given resolution, the ADM results are often more accurate than the CT results at early times, before the instabilities become apparent. We conclude with section IV. A study of the stability properties of the iterative Crank-Nicholson (ICN) scheme, used for the spacetime evolution of the simulations presented in this paper, can be found in the Appendix.

II. FORMULATION

We start reviewing briefly the formulations used for the comparisons.

The standard ADM equations are [15]:

$$\frac{d}{dt}\,\gamma_{ij} = -2\alpha K_{ij}, \tag{1}$$

$$\frac{d}{dt}\,K_{ij} = -D_iD_j\alpha + \alpha\Big(R_{ij} + KK_{ij} -2K_{ik}K^k{}_j - {}^{(4)}R_{ij}\Big), \tag{2}$$

with

$$\frac{d}{dt} = \partial_t - \mathcal{L}_\beta \tag{3}$$

and where $\mathcal{L}_\beta$ is the Lie derivative with respect to the shift vector β^i. Here R_{ij} is the Ricci tensor and D_i the covariant derivative associated with the three-dimensional metric γ_{ij}. The 4-dimensional Ricci tensor ${}^{(4)}R_{ij}$ is usually written in terms of the energy density ρ and stress tensor S_{ij} of the matter as seen by the normal (Eulerian) observers:

$${}^{(4)}R_{ij} = 8\pi\left[S_{ij} - \frac{1}{2}\left(S-\rho\right)\right]. \tag{4}$$

The conformal, trace-free reformulations of these equations make use of a conformal decomposition of the three-metric, and the trace-free part of the extrinsic curvature. Here we follow closely the presentation of Ref. [10]. The conformal three-metric $\tilde{\gamma}_{ij}$ is written as

$$\tilde{\gamma}_{ij} = e^{-4\phi}\gamma_{ij}, \tag{5}$$

with the conformal factor chosen to be

$$e^{4\phi} = \gamma^{1/3} \equiv \det(\gamma_{ij})^{1/3}. \tag{6}$$

In this way the determinant of $\tilde{\gamma}_{ij}$ is unity. The trace-free part of the extrinsic curvature K_{ij}, defined by

$$A_{ij} = K_{ij} - \frac{1}{3}\gamma_{ij}K, \tag{7}$$

where $K = \gamma^{ij}K_{ij}$ is the trace of the extrinsic curvature, is also conformally decomposed:

$$\tilde{A}_{ij} = e^{-4\phi}A_{ij}. \tag{8}$$

So far, these are just definitions of new variables, with no clear motivation for their introduction. Evolution equations for these new quantities are easy to find, and we summarize here the Baumgarte-Shapiro [10] discussion on these equations, but with an emphasis on the possible numerical implications of various choices one can make.

The evolution equations for the conformal three–metric $\tilde{\gamma}_{ij}$, and its related conformal factor ϕ are trivially written as

$$\frac{d}{dt}\tilde{\gamma}_{ij} = -2\alpha\tilde{A}_{ij}, \tag{9}$$

$$\frac{d}{dt}\phi = -\frac{1}{6}\alpha K. \tag{10}$$

The evolution equation for the trace of the extrinsic curvature K can easily be found to be

$$\frac{d}{dt}K = -\gamma^{ij}D_iD_j\alpha + \alpha\left[\tilde{A}_{ij}\tilde{A}^{ij} + \frac{1}{3}K^2 + \frac{1}{2}\left(\rho+S\right)\right], \tag{11}$$

where the Hamiltonian constraint was used to eliminate the Ricci scalar.

For the evolution equation of the trace-free extrinsic curvature $\tilde{A}_{ij}$ there are many possibilities. A trivial manipulation of Eq. (2) yields:

$$\frac{d}{dt}\tilde{A}_{ij} = e^{-4\phi}\left[-D_iD_j\alpha + \alpha\left(R_{ij} - S_{ij}\right)\right]^{TF} \tag{12}$$

$$+\alpha\left(K\tilde{A}_{ij} - 2\tilde{A}_{il}\tilde{A}^l_j\right), \tag{13}$$

but as shown previously [7,10] there are many ways to write several of the terms, especially those involving the Ricci tensor. For example, one could eliminate the Ricci scalar R again through the use of the Hamiltonian constraint.

With the conformal decomposition of the three–metric, the Ricci tensor now has two pieces, which we write as

$$R_{ij} = \tilde{R}_{ij} + R^\phi_{ij}. \tag{14}$$

The "conformal-factor" part R^{ϕ}_{ij} is given directly by straightforward computation of derivatives of ϕ:

$$R^{\phi}_{ij} = -2\tilde{D}_i\tilde{D}_j\phi - 2\tilde{\gamma}_{ij}\tilde{D}^l\tilde{D}_l\phi \qquad (15)$$

$$+4\tilde{D}_i\phi\,\tilde{D}_j\phi - 4\tilde{\gamma}_{ij}\tilde{D}^l\phi\,\tilde{D}_l\phi, \qquad (16)$$

while the "conformal" part $\tilde{R}_{ij}$ can be computed in the standard way from the conformal three–metric $\tilde{\gamma}_{ij}$. To simplify notation, it is convenient to define what Ref. [10] calls the "conformal connection functions":

$$\tilde{\Gamma}^i := \tilde{\gamma}^{jk}\tilde{\Gamma}^i_{jk} = -\tilde{\gamma}^{ij}{}_{,j}, \qquad (17)$$

where the last equality holds if the determinant of the conformal three–metric $\tilde{\gamma}$ is actually unity (notice that this should be true analytically, but may not be numerically).

Using the conformal connection function, the Ricci tensor can be written:

$$\tilde{R}_{ij} = -\frac{1}{2}\tilde{\gamma}^{lm}\tilde{\gamma}_{ij,lm} + \tilde{\gamma}_{k(i}\partial_{j)}\tilde{\Gamma}^k + \tilde{\Gamma}^k\tilde{\Gamma}_{(ij)k}$$
$$+\tilde{\gamma}^{lm}\left(2\tilde{\Gamma}^k_{l(i}\tilde{\Gamma}_{j)km} + \tilde{\Gamma}^k_{im}\tilde{\Gamma}_{klj}\right). \qquad (18)$$

Here again, one has choices in how the terms involving the conformal connection functions $\tilde{\Gamma}^i$ are computed. A straightforward computation based on the Christoffel symbols could be used (and usually is in standard ADM formulations), but this approach leads to derivatives of the three–metric in no particular elliptic form. One would like to see an elliptic form as the principal part of this expression, as it brings the $\tilde{\gamma}_{ij} - \tilde{A}_{ij}$ system a step closer to being hyperbolic. Thanks to the definition of the $\tilde{\Gamma}^i$'s, an explicitly elliptic operator is singled out. However, if the terms involving the $\tilde{\Gamma}^i$ are evaluated directly in terms of derivatives of the three–metric, this elliptic operator serves no special purpose, as other second derivatives appear through derivatives of the $\tilde{\Gamma}^i$ which spoils the elliptic nature of the operator as a whole. If, on the other hand, the $\tilde{\Gamma}^i$ are promoted to independent variables, for which evolution equations can be derived, then the expression for the Ricci tensor retains its elliptic character. The price to pay is that one must now evolve three additional quantities in the evolution system. Whether this has any numerical advantage will depend on details of the implementation, and will be discussed below.

Following this argument of promoting the $\tilde{\Gamma}^i$ to independent variables, it is straightforward to derive their evolution equation:

$$\frac{\partial}{\partial t}\tilde{\Gamma}^i = -\frac{\partial}{\partial x^j}\Big(2\alpha\tilde{A}^{ij} + 2\tilde{\gamma}^{m(j}\beta^{i)}{}_{,m}$$
$$-\frac{2}{3}\tilde{\gamma}^{ij}\beta^l{}_{,l} - \beta^l\tilde{\gamma}^{ij}{}_{,l}\Big). \qquad (19)$$

However, again there is a choice one can make in writing this evolution equation; as pointed out in Ref. [10] it turns out that the above choice leads to an unstable system. A choice which will be shown to be better can be obtained by eliminating the divergence of $\tilde{A}^{ij}$ with the help of the momentum constraint:

$$\frac{\partial}{\partial t}\tilde{\Gamma}^i = -2\tilde{A}^{ij}\alpha_{,j} + 2\alpha\Big(\tilde{\Gamma}^i_{jk}\tilde{A}^{kj} -$$
$$\frac{2}{3}\tilde{\gamma}^{ij}K_{,j} - \tilde{\gamma}^{ij}S_j + 6\tilde{A}^{ij}\phi_{,j}\Big)$$
$$+\frac{\partial}{\partial x^j}\Big(\beta^l\tilde{\gamma}^{ij}{}_{,l} - 2\tilde{\gamma}^{m(j}\beta^{i)}{}_{,m} + \frac{2}{3}\tilde{\gamma}^{ij}\beta^l{}_{,l}\Big). \qquad (20)$$

With this reformulation, in addition to the evolution equations for the conformal three–metric $\tilde{\gamma}_{ij}$ (9) and the conformal-traceless extrinsic curvature variables $\tilde{A}_{ij}$ (13), there are evolution equations for the conformal factor ϕ (10), and the trace of the extrinsic curvature K (11). If the $\tilde{\Gamma}^i$ are promoted to the status of fundamental variables, as in Ref. [10], they can be evolved with (20). (Note that the mixed first and second order evolution system for $\{\phi, K, \tilde{\gamma}_{ij}, \tilde{A}_{ij}, \tilde{\Gamma}^i\}$ is not in any immediate sense hyperbolic [16]). In the original formulation of Shibata and Nakamura [7], the auxiliary variables $F_i = -\sum_j \tilde{\gamma}_{ij,j}$ are used instead of the $\tilde{\Gamma}^i$, and the final system of equations is somewhat more complicated.

Ref. [17] shows that the CT system can also be interpreted as a "conformal second-order" version of the Bona-Massó system with $2V_i = -(\tilde{\Gamma}_i + 8\partial_i\phi)$.

A. Slicings

Systems of the CT type have been investigated with various slicing conditions in the past. The paper of Baumgarte and Shapiro considered geodesic and harmonic slicing, while earlier work by Shibata and Nakamura, and the more recent paper by Baumgarte, Hughes, and Shapiro [11] have also considered maximal slicing. Here we have studied maximal slicing and a number of algebraic slicings, and used them with different implementations of the CT equations, on numerical evolutions of many different spacetimes.

Maximal slicing has the property that $K = 0$, leading to an elliptic equation for the lapse

$$\nabla^2\alpha = \alpha\left[K_{ij}K^{ij} + 4\pi\left(\rho + S\right)\right]. \qquad (21)$$

Notice that in maximal slicing the evolution equations for ϕ and K become simply

$$d\phi/dt = 0, \quad dK/dt = 0. \qquad (22)$$

The algebraic slicings that we will consider here correspond to the family originally introduced by Bona and Massó [18], building on earlier work of Bernstein [19]

$$\mathcal{L}_t\,\alpha = -f(\alpha)\alpha^2 K, \qquad (23)$$

with $f(\alpha) > 0$ but otherwise arbitrary. This family contains many well known slicing conditions. For example, taking $f = 1$ we recover the "harmonic" slicing condition, which after a trivial integration becomes

$$\alpha = F(x^i) + \gamma^{1/2}, \tag{24}$$

with F an arbitrary function of space. The name "harmonic" slicing comes from the fact that it corresponds to the choice of a harmonic time coordinate

$$\Box t = 0. \tag{25}$$

Another useful slicing condition is obtained by taking $f = N/\alpha$. This corresponds to the generalized "1+log" slicing condition [17] which after integration becomes

$$\alpha = F(x^i) + \log \gamma^{N/2}. \tag{26}$$

(There is in fact some inconsistency in terminology as to whether the $N = 1$ or the $N = 2$ case corresponds to the standard "1+log" slicing; different choices being made by different authors.)

These type of algebraic slicings have an advantage over maximal slicing in terms of computational efficiency: It is much faster to integrate an evolution equation for the lapse than to solve an elliptic equation. On the other hand, such algebraic slicings are prone to the development of gauge pathologies [20,21]. The possibility of the appearance of such pathologies when using algebraic slicings should always be kept in mind, as a gauge pathology can easily be confused with a numerical instability: one can lose a lot of sleep trying to cure an "instability" that is in fact a true solution of our system of differential equations.

B. Boundary conditions

In standard 3+1 numerical simulations, the computational domain covers only a finite region of space. One must therefore apply some sort of artificial boundary condition at the edges of the numerical grid. Ideally, one would like to find a boundary condition that does not introduce numerical instabilities and allows gravitational waves to leave the grid cleanly, with no artificial reflections. This is in itself a very difficult problem, since in the first place, there is no local boundary condition that allows waves coming from any arbitrary direction to leave the grid with no reflections, and second, there does not even exist a clear way to define what a wave is in general relativity except at asymptotic infinity. In practice, what one looks for is a condition that remains stable and allows some "wave-like" solutions to leave the grid without introducing large reflections at the boundaries. The amount of artificial reflection that results typically depends on the specific form of the boundary condition, and on the direction of motion of the wave fronts as they hit the boundary [22].

Since in this paper we are interested in the question of the stability of the interior evolution, we will not worry too much about the boundary conditions, and we will limit ourselves to describing a few conditions that we have found to work well in practice. The conditions we have used are the following:

- Static boundary condition: The evolved variables are simply not updated at the boundary, and remain with their initial values there. This condition is very bad at handling waves since it reflects everything back in, but it can be very useful when studying situations that are supposed to remain static (as are some of the systems studied below), and where all the dynamics comes from numerical truncation errors.

- Zero-order extrapolation or "flat" boundary condition: After evolving the interior, the value of a given variable at the boundary is simply copied from its value one grid point in (along the normal direction to the boundary). This condition allows for some dynamics at the boundaries, and is somewhat better at absorbing waves than the static boundaries, but it still introduces a considerable amount of reflections.

- Sommerfeld or "radiative" boundary condition: In this case we assume that the dynamical variables behave like a constant plus an outgoing radial wave at the boundaries, that is:

  $$f(x^i, t) = f_0 + u(r - t)/r, \tag{27}$$

  where $r = \sqrt{x^2 + y^2 + z^2}$ and where the constant f_0 is taken to be one for diagonal metric components and zero for everything else. The radiative condition assumes that the boundaries are in the wave zone, where the speed of light is essentially one, and where the gravitational waves behave as spherical wavefronts. This boundary condition has been used before by other authors [7,10], and it has been found that in practice it is very good at absorbing waves.

  It is in fact easier to implement a differential form of the radiative boundary condition than to use (27) directly. Consider a boundary that corresponds to a coordinate plane x_i=constant. Condition (27) then implies:

  $$\frac{x_i}{r}\,\partial_t f + \partial_i f + \frac{x_i}{r^2}\,(f - f_0) = 0. \tag{28}$$

  One can now use simple finite differences to implement this last condition. In our code we have implemented condition (28) consistently to second order in both time and space.

- Robin boundary condition: This is a different type of "extrapolating" boundary condition, where one assumes that for large r a given field behaves as:
$$f(x^i) = f_0 + k/r, \tag{29}$$
with k constant. This condition is clearly related to the radiative condition described above, but it contains no information about the time evolution. Just as we did with the radiative condition, we in fact implement the Robin condition in differential form:
$$\partial_i f + \frac{1}{r}\ (f - f_0) = 0. \tag{30}$$
The Robin boundary condition is usually better suited for solving elliptic problems than for use on dynamical variables.

Most of the simulations discussed below have been performed using the radiative boundary condition (28) for the dynamical variables, and the Robin boundary condition (30) both for constructing the initial data and for solving the maximal slicing condition. Whenever a different boundary condition is used, we say so explicitely.

III. APPLICATIONS

In this section we will apply the previous system of conformal trace-free equations, exploring different implementations, in a series of numerical experiments with different spacetimes. The various implementations we consider are:

- Promoting the Γ's to independent variables.
- Use the momentum constraints on the evolution equation for the Γ's.
- Enforcing $\mathrm{tr}\tilde{A} = 0$.
- For maximal slicing, enforcing $\mathrm{tr}K = 0$.

We will study the effects of these different implementations using strong gravitational waves spacetimes.

All the numerical simulations presented here are carried out with the Cactus code for numerical relativity co-developed in our NCSA/Potsdam/Wash U collaboration and elsewhere.

A. Vacuum Spacetimes

We begin our discussion of the numerical simulations with vacuum spacetimes in this subsection, examining the evolution of both strong gravitational wave and black hole spacetimes. In particular, we use the gravitational wave simulations to illustrate the effects of the various implementations of the CT approach.

1. Pure Gravitational Waves

We first turn to pure gravitational wave spacetimes. The low amplitude linear case has been studied, with a full 3D code, and published previously, (a) in both the standard ADM formulation and the Bona-Massó hyperbolic formulation by [23], where no fundamental differences were seen in performance at that time, and (b) by Shibata and Nakamura [7] and Baumgarte and Shapiro [10] in the CT approach as described above. The Baumgarte and Shapiro [10] work particularly showed the strength of the CT formulation in the linearized case. Here we extend the study of these systems to include highly dynamic, strong field regimes. The study here is limited to tests that show the strengths and weaknesses of the different formulations. A study of the physics of collapsing waves in full 3D numerical relativity is presented elsewhere [24].

We consider here a three–metric of the form originally considered by Brill [25]:
$$ds^2 = \Psi^4 \left[e^{2q}\left(d\rho^2 + dz^2\right) + \rho^2 d\phi^2 \right] = \Psi^4 \hat{ds}^2, \tag{31}$$
where q is a free function subject to certain regularity and fall-off conditions. Different forms of the function q have been considered by different authors [26–29], but most work so far has concentrated only in constructing and analyzing the initial data.

As in Ref. [24], we use a generalized form for the function q, giving it a full 3D dependence, following [30–33]:
$$q = a\ \rho^2\ e^{-r^2} \frac{(1 + c\rho^2 \cos^2(\mathrm{m}\theta))}{(1 + \rho^2)}, \tag{32}$$
where a and c are constants, $r^2 = \rho^2 + z^2$ and m is an integer. In this paper we focus on the axisymmetric case, $c = 0$, for simplicity, although using a non-zero value of c does not affect the results we discuss below. All the runs discussed here where performed using an iterative Crank-Nicholson (ICN) scheme with 3 iterations (see appendix), and radiative boundary conditions.

The first case presented is an initial configuration with amplitude a=4, corresponding to a strong wave, but not quite strong enough to collapse to a black hole. In the evolution of this data set the wave implodes through the origin, oscillates a few times, and finally disperses back to infinity leaving flat space behind, but in a non-trivial spatial coordinate system [24]. The evolution of this spacetime is highly non-linear, and the final configuration has metric components with a large dynamical range.

In Fig. 1a we show the evolution of the minimum value of the lapse over the grid for a simulation done with the standard ADM formulation, using maximal slicing, no shift and a radiative boundary condition. For this particular simulation we used a resolution of Δx=0.08 and 67^3 grid points. Also, we used the fact that our data

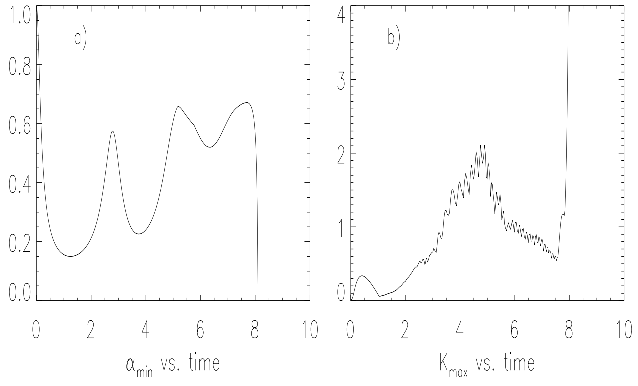

FIG. 1. a) Evolution of the minimum value of the lapse for an axisymmetric Brill wave data set with a=4, using the standard ADM formulation with maximal slicing. The simulation crashes at t=8 with a catastrophic collapse of the lapse. b) Evolution of the maximum value of the trace of the extrinsic curvature K.

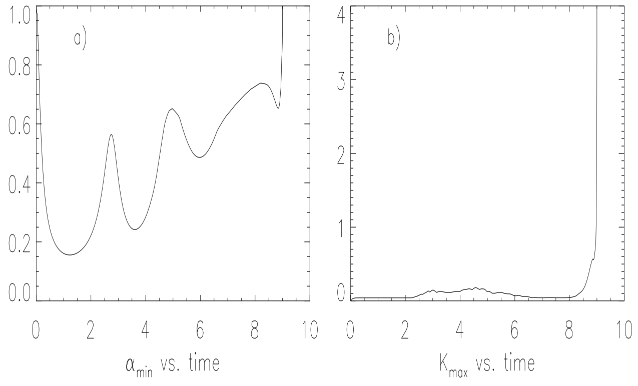

FIG. 2. a) Evolution of the minimum value of the lapse for an axisymmetric Brill wave data set with a=4, using the standard ADM formulation with maximal slicing and a K-driver. The simulation goes somewhat further, and now crashes at t=9 with a catastrophic blow-up of the lapse. b) Evolution of the maximum value of the trace of the extrinsic curvature K. The trace now remains much smaller during the simulation.

is symmetric across coordinate planes to evolve only one octant. The simulation crashes at $t \simeq 8$ when the lapse collapses catastrophically in response to a blow up of the extrinsic curvature. Fig. 1b shows the evolution of the maximum value of the trace of the extrinsic curvature K. Notice that even though we are using maximal slicing, K does not remain zero, and blows up towards the end of the simulation. The fact that K does not remain zero is not surprising, since the maximal slicing condition is solved numerically, and thus a residual time derivative of K is to be expected. The catastrophic blow-up, however, is a different matter and points towards the existence of an unstable solution of our system of equations.

Fig. 2 shows the same simulation, but now using the so-called "K-driving" technique [34]. The idea here is to add counter terms to the elliptic equation for the lapse to drive the numerically produced non-zero K (the trace of the extrinsic curvature) back towards zero. With K-driving, K remains much smaller until close to the point of crashing at t=9, with a catastrophic blow-up of the lapse at the end. This shows that a better control of the time slicing is not enough to cure the instability in the evolution: There exist unstable modes that are not controlled by keeping the value of K small. (For an analysis of possible unstable modes of the ADM equations, see [4].)

Next, we show the evolution of the same system using again maximal slicing, and different implementations of the CT formulation. In Fig. 3 we show again the central value of the lapse for the same initial data. The different runs correspond to the following cases:

	use of Γ^i	use momentum constraints	force K=0	remove tr$\tilde{A}$
Res	no	-	no	no
Gam	yes	no	no	no
Mom	yes	yes	no	no
AFK	yes	yes	yes	no
AFA	yes	yes	no	yes
AF2	yes	yes	yes	yes

The first run uses the implementation denoted "Res" (for rescale). It differs from the standard ADM equations only in the conformal rescaling and the fact that ϕ and K (which enter into the evolution equation for $\tilde{A}_{ij}$) are now evolved separately. The second run, with the implementation denoted "Gam" (for gamma), introduces the Γ^i, but does not use the momentum constraints to rewrite their evolution equations. The third run uses the implementation "Mom" (for momentum constraints) and represents a straightforward coding of the the full set of CT equations [7,10], where the momentum constraints are used to modify the evolution equations for the Γ^i, but without adding anything else. In the fourth run, which uses the implementation "AFK" (for "actively enforcing K"), we have forced K to remain zero by simply not evolving it, and we have also kept ϕ time independent (see Eq. (10)). In the fifth run we use the implementation "AFA", where we allow K to evolve freely, but actively force $\tilde{A}$ (the trace of $\tilde{A}_{ij}$) to remain zero by subtracting it from $\tilde{A}_{ij}$ after each time step:

$$\tilde{A}_{ij} \leftarrow \tilde{A}_{ij} - \frac{1}{3}\tilde{\gamma}_{ij}\ \mathrm{tr}\tilde{A}. \tag{33}$$

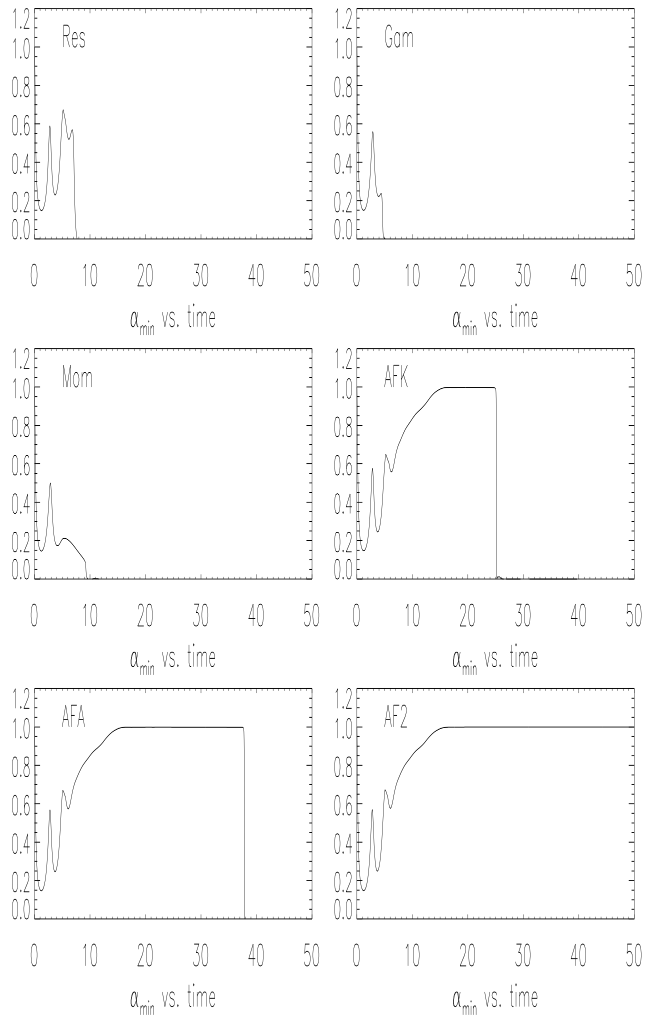

FIG. 3. Evolution of the minimum value of the lapse for an axisymmetric Brill wave data set with a=4, using the 6 different variations of the CT system described in the text.

And finally, in the sixth run we use the implementation "AF2" that combines implementations AFK and AFA above by actively enforcing both K=0 *and* $\tilde{A}$=0. Notice that both K and $\tilde{A}$ should be zero in principle in an exact evolution using the CT equations with maximal slicing, but they do not remain so in actual numerical evolutions unless actively enforced.

As can be seen from the figure, runs Res, Gam, Mom, AFK and AFA eventually crash, but run AF2 with double active enforcement does not, at least for the time scale under study. The lapse returns to unity, and the final static spacetime can be followed for a long time with no sign of an instability (we have in fact followed run AF2 past t=100 and it still remains stable). From the figure we also see that by enforcing only K=0 or A=0 separately, as is done in runs AFK and AFA, one still obtains improved stability, with the simulations crashing at late times after the lapse has already returned to 1. This shows that by enforcing only one of the two constraints, and keeping the other options turned on, we still get a rather robust system when compared to standard ADM. Moreover, enforcing $\tilde{A}$=0 appears to be more important than enforcing K=0, as can be seen from the fact that run AFA crashes much later than run AFK.

Finally, notice that run Gam crashes even sooner than run Res, which shows that it is in fact better not to use the Γ^i than to use them without modifying their evolution equation. For understanding the need to use the momentum constraints in the CT approach, see the companion paper [4].

We note that the results found above for the different implementation are generic for strong gravitational wave spacetimes, quite independent of the precise parameter choices. However, for weak gravitational waves in the linear regime, the straightforward coding of the CT equations (implementation "Mom") leads also to stable evolutions as do the AFK, AFA and AF2 cases. In Fig. 4 we show again the minimum value of the lapse for the evolution of a wave with an amplitude of $a = 0.01$, using the ADM formulation and also the Mom, AFK and AFA implementations of the CT system (since the lapse remains very close to 1, we are in fact plotting $(\alpha - 1) \times 10^5$). We see that while the ADM run crashes at an early time ($t \simeq 15$) with a catastrophic collapse of the lapse, all three implementations of the CT equations give stable evolutions and yield basically the same results for a weak wave. We have followed these three runs past t=100 with no instabilities developing (the AF2 implementation is in fact just as stable, but we don't include it in the figure).

From these studies (and many others with different parameters that we have done) we can conclude that, for maximal slicing, the CT formulation has better stability properties for the evolution of strong field systems, as long as:

- The Γ^i are promoted to independent variables.
- The momentum constraints are used to transform the evolution equation for the Γ^i. Evolving the Γ^i without modifying their evolution equation is worse than not using them at all.
- The trace of the extrinsic curvature K is actively forced to be zero (the definition of maximal slicing).
- The trace of the $\tilde{A}_{ij}$ is also actively forced to be zero.

So far we have focused on the issue of long term stability. Now we want to compare accuracy of the CT and ADM formulations. We concentrate on the best implementation of the CT equations, the one we labelled AF2. In Fig. 5 we show the L2-norms of the hamiltonian constraint for the a=0.01 and a=4 cases discussed above, using the ADM (solid line) and the AF2 systems (dashed

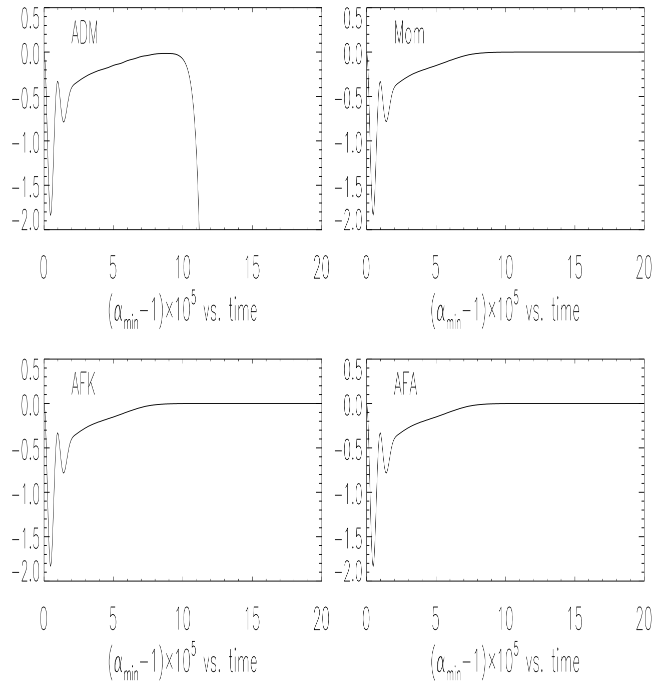

FIG. 4. Evolution of the minimum value of the lapse for an axisymmetric Brill wave data set with a=0.01 for the ADM system and three variations of the CT system (Mom, AFK, AFA). Notice that since the lapse remains very close to 1, we are in fact plotting $(\alpha - 1) \times 10^5$.

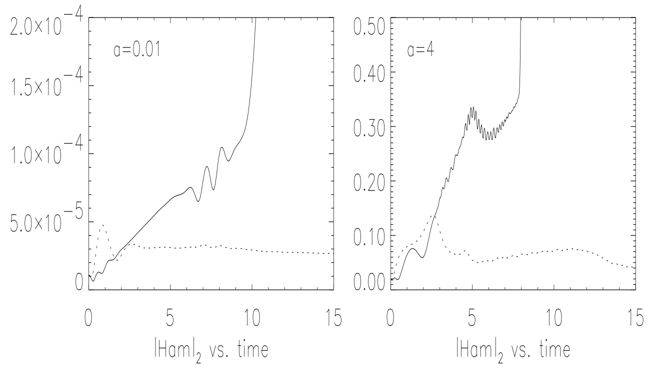

FIG. 5. L2-norms of the hamiltonian constraint for the a=0.01 and a=4 cases, using the ADM (solid line) and the AF2 systems (dashed line).

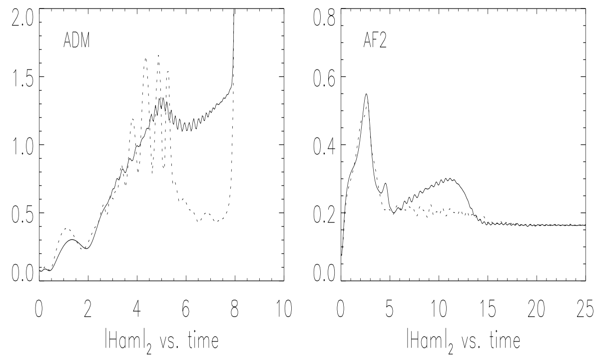

FIG. 6. Convergence of the L2-norms of the hamiltonian constraint for the a=4 case for both the ADM and the AF2 systems. The dashed lines show the L2 norm for a resolution for of 0.16, while the solid lines show the L2 norm for a resolution for of 0.08 multiplied by a factor of four.

line). In both cases we see that for the ADM system, the L2-norm of the hamiltonian constraint grows more or less linearly for some time (this is more evident in the a=0.01 case) until just before the crash when it blows up catastrophically. In contrast, in the AF2 runs the L2-norm of the hamiltonian constraint initially grows faster, but it later settles on a constant value. The fact that the ADM runs are more accurate than the AF2 runs at early times appears to be quite generic: we have found essentially the same behavior for all the different parameters that we have studied.

We have also performed convergence tests by running the same initial data with different resolutions, and we have found that both the ADM and AF2 evolutions are second order accurate. As an example of this, Fig. 6 shows the L2-norms of the hamiltonian constraint for both the ADM and the AF2 systems for two different resolutions: The dashed lines show the L2 norm for a resolution of dx=0.16 (35^3 grid points), while the solid lines show the L2 norm for a resolution of dx=0.08 (67^3 grid points) multiplied by a factor of four. For second order convergence the solid and dashed lines should fall on top of each other. From the figure we see that this is indeed true for most of the run in both cases. For the ADM run, second order convergence starts to fail shortly before the crash. On the other hand, for the AF2 run we obtain slightly degraded convergence (but still better than first order) for times between t=5 and t=15 when the spacetime is very dynamic, indicating that we haven't quite reached the second order convergence regime for the resolutions considered here.

Though in this section we have concentrated in the case of maximal slicing, we should mention that we have also performed many simulations using the generalized "1+log" slicings. The results are in fact very similar to those reported here, except for the fact that implementations AFK and AF2 can no longer be used (since K in non-zero for these slicing conditions). We find that for these algebraic slicings, implementation AFA is by far the best performer.

In the following subsections, we show that the above results on the stability and accuracy of the ADM and CT systems are basically the same for systems ranging from black holes to spacetimes coupled to dynamical source fields.

2. Black Holes

Black holes have been the target of an intense research effort in recent years in numerical relativity, and have proved particularly difficult to handle in 3D evolutions. In the "standard" numerical evolution of black holes using the ADM equations together with singularity avoiding slicings, 3D simulations generally develop instabilities and crash before $t = 50M$, where M is the mass of the system [35–37]. This falls far short of the time required to model the complete inspiral of two black holes, or even the head-on collision. Still, singularity avoiding slicings combined with the ADM equations make it possible to evolve through a brief part of the merger phase of two black holes with momenta and spins, and from this point of view give the most generally applicable method available. Future cures for grid stretching are expected to be based on black hole excision [38,39] or characteristic slicings [40].

In the following we carry out a preliminary study of the CT formulation in black hole evolutions with grid stretching. It is inevitable that the sharp peaks that develop in the metric function due to grid stretching will cause the code to crash at some point in the evolution. We consider the evolution of the Misner data as a concrete example. The 3D numerical evolution of the Misner data in the standard ADM setting with singularity avoiding slicing has previously been studied using the so-called "G" code [36,30] and its derivatives [35], developed by the NCSA/WashU group. Comparable results for a single black hole can be found in [17].

In Fig. 7 and Fig. 8 we compare the results of evolutions of Misner data with the separation parameter $\mu = 2.2$, corresponding to two initially well separated black holes, on a grid of size 130^3 with grid spacing 0.08. The only difference in the simulations is the system of equations used to carry out the evolution (ADM vs. AF2); all computational parameters, such as parameters in the ICN finite differencing scheme, grid parameters, radiative boundary conditions, and maximal slicing condition are the same. In Fig. 7, first panel, we show the radial-radial metric component along a line on the equatorial plane at various times for the ADM case. We can clearly see the familiar ever-growing peak caused by the grid stretching associated with singularity avoiding slicings. In the first panel of Fig. 8 we show the lapse function along a line on the equatorial plane at various times for the ADM case, and here an instability becomes apparent at around $t = 14M$ which is not yet reflected in the metric. This short wave length instability grows rapidly and causes the code to crash at $t = 14M$. In the

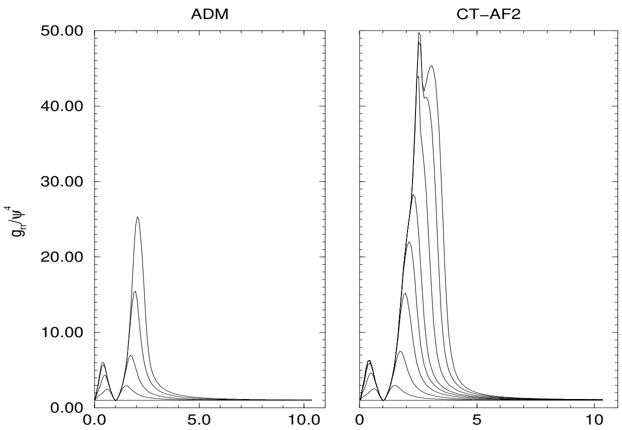

FIG. 7. Evolution of the radial-radial metric component along a line on the equatorial, plane at various times for Misner data ($\mu = 2.2$). Plots are every $3.5M$ in time. The ADM system crashes after $t = 14M$, while the AF2 system remains stable.

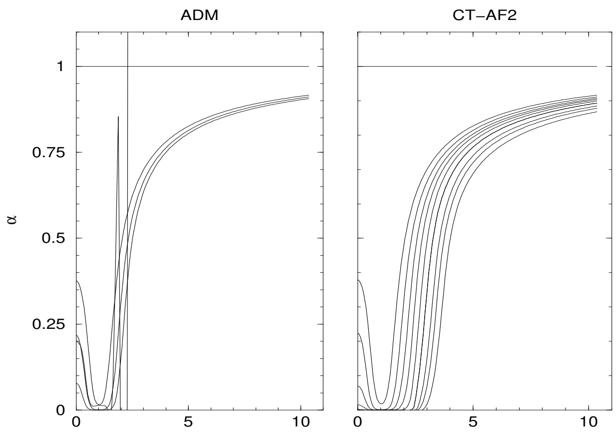

FIG. 8. Evolution of the lapse function along a line on the equatorial plane at various times for Misner data ($\mu = 2.2$). Plots are every $3.5M$ in time. The ADM system crashes after $t = 14M$, while the AF2 system remains stable.

second panel we show the AF2 case. No metric instability is seen until towards the end of the simulation at $t = 24M$, although the peak appears to be deformed. At this time the radial metric function peak has grown to about two times higher than that attained in the ADM case. The lapse for the AF2 case in Fig. 8 does not show an instability.

However, note that a smooth and stable evolution of the lapse does not mean that the computed data is still useful. To emphasize this point, Fig. 9 shows the same run as above with AF2 on a smaller grid with only 66^3 points, but with the same grid spacing as before (so the boundaries are much closer in). While ADM crashes when the gradients in the metric become too severe, the AF2 run is able to continue with a smooth lapse even after the metric becomes deformed (cmp. [17] where the evolution of the metric is not discussed). The lapse eventually collapses in the whole grid, freezing the evolution

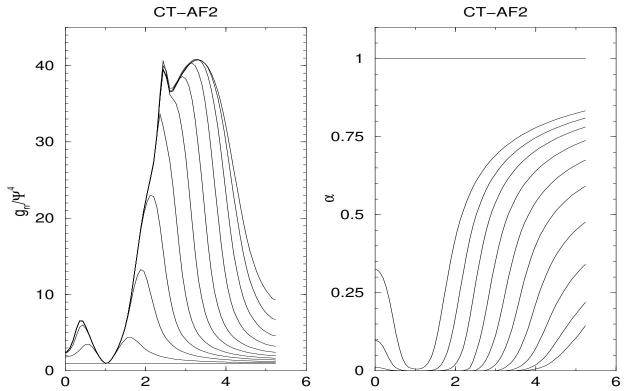

FIG. 9. Evolution of the lapse and the metric at various times for Misner data ($\mu = 2.2$). Plots are every $5M$ in time. With the AF2 system the evolution remains stable even after the metric peak is severely deformed.

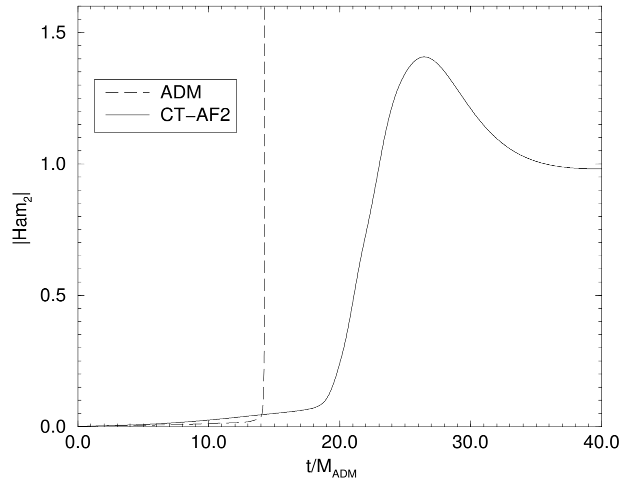

FIG. 10. Evolution of the L2-norm of the Hamiltonian constraint for Misner data ($\mu = 2.2$). The ADM system crashes at around $t = 14M$, while the AF2 remains stable. However, the accuracy of the AF2 run degrades significantly after around $t = 20M$.

(so one could keep running "forever", but the evolution becomes meaningless).

Next, we compare the accuracy of both simulations. In Fig. 10 we show the L2 norm of the Hamiltonian constraint for a grid size of 130^3. The dashed line represents the ADM run, and the solid line the AF2 run. We see that the ADM results are more accurate than the AF2 results until just after time $t = 14M$, when the instability in the ADM evolution begins to dominate and the code crashes (with higher resolution this crash time can be delayed somewhat). Starting at around $t = 20M$ for AF2, there is a spurious growth in the Hamiltonian constraint that corresponds to the deformation in the metric. For maximal slicing one expects continuous growth of a smooth metric peak, but with AF2 the shoulder in the lapse seems to overtake the outward movement of the metric peak, freezing its growth in an irregular manner.

These results for black holes with grid stretching cannot be compared directly to the wave runs in the previous section because in the case of the black hole runs we do not approach a static final state. However, the CT formulation still offers some advantages over ADM in achievable run time. We find stability far beyond were the runs are meaningful, and it remains to be explored how far one can push the CT runs while maintaining convergence.

B. Matter Spacetimes

In the previous sections we studied the stability properties of the vacuum Einstein equations. What will happen if these equations are coupled to dynamical matter sources that are themselves governed by evolution equations coupled to the spacetime geometry? The complete set of equations can now have more complicated types of unstable modes. What would be the effects of switching from the ADM formulation to the CT formulation?

To respond to this question we consider next the following systems: (i) the evolution of boson stars governed by the scalar field Klein-Gordon equation and (ii) the evolution of neutron stars governed by the hydrodynamical equations (general relativistic Euler equations). The numerical evolution of the Klein-Gordon equation is straightforward with many well-known stable schemes. However, the numerical evolution of the hydrodynamical equations is considerably more challenging, especially in the presence of shocks or highly relativistic flows. For this purpose we use a recently developed hydrodynamical code [41] which employs a conservative formulation of the equations together with high-resolution shock-capturing (HRSC) schemes based on approximate Riemann solvers. In [41] we demonstrated that this code is capable of handling hydrodynamical evolutions in a stable and accurate fashion for a range of scenarios.

We focus here on analyzing the stability and accuracy of evolutions of both static boson stars and static neutron stars using the ADM formulation and the AFA implementation of the CT equations discussed above. We use the AFA implementation rather than AF2 because the simulations discussed here have all been performed using algebraic slicings and implementation AF2 applies only to maximal slicing. The main motivation for this has been the fact that, as we will show below, implementation AFA with algebraic slicings already gives excellent results when compared with standard ADM and is far less computationally expensive than runs that use maximal slicing.

1. Boson Stars

We begin with a simple kind of matter source: self-gravitating scalar fields. This system has served as a useful testbed for developing numerical techniques for dealing with relativistic matter coupled to the Einstein equations [42,34,43,44], and also has a distinguished history in the field, having provided the first example of critical phenomena in relativity [45].

The dynamics of a massive scalar field are described by the minimally coupled Klein-Gordon (KG) equation

$$\Box_g \phi = m^2 \phi, \tag{34}$$

(see, e.g. [42]). The KG equation can be obtained from the Lagrangian

$$\mathcal{L} = \frac{1}{2} g^{\mu\nu} \phi,_\mu \phi^*,_\nu + \frac{1}{2} m |\phi|^2, \tag{35}$$

which leads to the stress-energy tensor

$$T_{\mu\nu} = \frac{2}{\sqrt{-g}} \frac{\delta \mathcal{L}}{\delta g^{\mu\nu}}, \tag{36}$$

which is used as the matter source for the Einstein equations.

Self-gravitating massive scalar fields have bound, star-like solutions called boson stars with stability properties very much like those of neutron stars. These objects have been studied numerically, extensively in 1D [42,44] and also in 3D [34]. Apart from the fact that their evolution equation is much simpler than the hydrodynamical equations, boson stars are also easier to handle numerically when compared to neutron stars because they have no sharp changes in the density distribution near the surface layer of the star. For more details on the properties of boson stars and their behavior under perturbations see [42] and references cited therein.

We perform our numerical evolutions of boson stars by writing the KG equation as a flux-conservative system of the form

$$\dot{u}_a = \partial_b F^b_a + S^b_a u_b \tag{37}$$

where $\vec{u}$ contains the scalar field and its time and space derivatives. The method used to integrate this equation is a symmetrized MacCormack with both directional and Strang splitting. Symmetrized here means that the order of left-hand and right-hand differencing changes every time step (this improves the stability of the scalar field evolution). The code for solving the KG equation converges to second order in time and space. See Ref. [46,47] for details of the numerical methods.

We have carried out evolutions of equilibrium boson star configurations with the metric background held fixed artificially (not updating the metric functions), and evolutions of the metric of such configurations with the scalar field held fixed artificially (not updating the scalar field), for a range of compactness of the boson stars, using both the ADM and AFA schemes. For all these cases, we have seen that the simulations are stable and second order convergent. The case of coupled spacetime-scalar field evolution is much more challenging, and we focus on that below.

We begin by showing an equilibrium boson star with a central density near the maximum stable value (field strength at center $\phi_0 = 0.26$, total mass $M = 0.6322\ {m_p}^2/m$, with m_p the Planck mass, m the mass of the scalar field). In Fig. 11, we show the evolution of radial metric component g_{rr} in a fully coupled simulation, using a three step ICN scheme, 1+log slicing with $N = 2$, no shift, a radiative boundary condition on the metric, and a flat boundary condition on the scalar field. A 32^3 grid is used to cover only one octant. In the first panel we show the results of the ADM evolution. We see that for a short time, the spacetime remains nearly static (as it should). However, a short wavelength instability becomes significant by time t=7, and quickly grows causing the code to crash. The time t here is expressed in terms of the intrinsic oscillation time scale of the scalar field (the exact equilibrium boson star field has the form $\psi(r)e^{it}$). In the second panel we show the evolution with exactly the same setup but using now implementation AFA instead of ADM. We see that the static configuration is maintained for a much longer time. Towards the end of the evolution, near $t = 150$, we see that numerical error starts to build-up near the boundary of the computational domain.

In Fig. 12 below, we compare the L2-norm of the hamiltonian constraint for the ADM and AFA runs. We see that at early times the ADM run gives a more accurate result, but instabilities cause the L2-norm to blow by $t \simeq 8$. For the AFA run the constraint violation is larger at first, but the evolution remains stable or a much longer time. The oscillation of the hamiltonian constraint we see here can be understood as a reaction of the scalar field to the numerical truncation error, which can be interpreted as a kind of perturbation. The frequency of these oscillations coincides with the ones obtained in 1D studies of perturbed boson stars. Notice that with the ADM run the code crashes so early that one can not even see the first oscillation.

2. Static Neutron Stars

We turn now to the study of hydrodynamical evolutions of neutron stars. In [41] we developed a three-dimensional, fully relativistic code to integrate the hydrodynamical equations coupled to the ADM equations. Convergence studies using polytropic neutron stars showed that the code is second order accurate in both

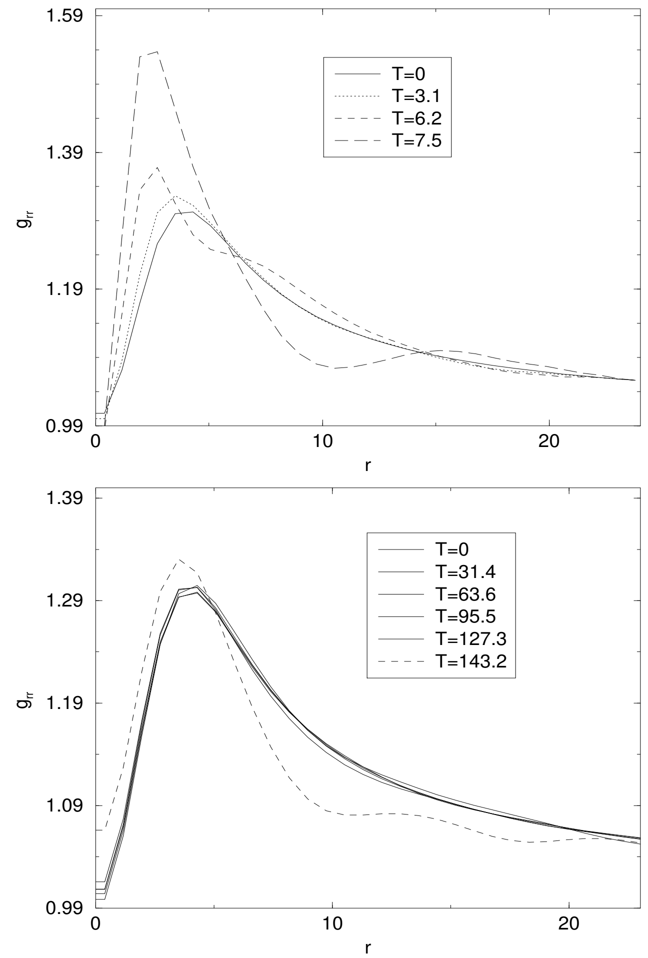

FIG. 11. Evolution of the radial metric function g_{rr} using ADM (upper panel) and the AFA implementation (lower panel). The ADM evolution crashes at $t \simeq 8$.

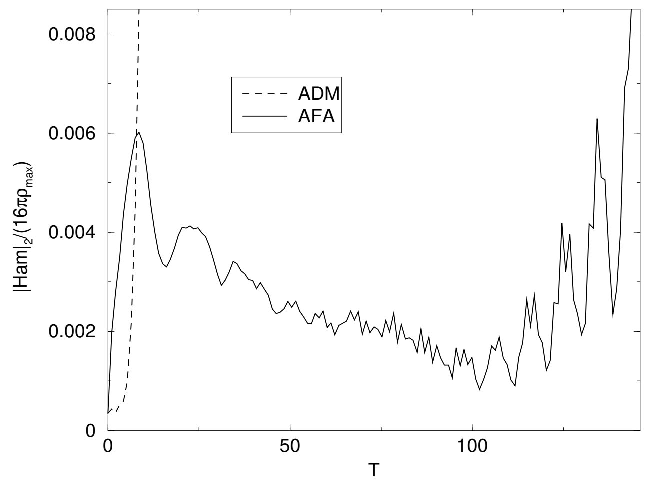

FIG. 12. Evolution of the L2-norm of the Hamiltonian constraint for a static and stable fully coupled boson star using the ADM and AFA systems. The evolutions where carried out on a 32^3 grid, with a resolution of $\Delta x = 0.45$.

space and time. For the integration of the hydrodynamical equations we used HRSC schemes of the total-variation-diminishing (TVD) class, with a piecewise-linear reconstruction of a sufficient set of hydrodynamical variables (rest-mass density, three-velocity and internal energy density). For more details on the schemes available in the code, see [41]. In the studies reported in this paper we use the ICN scheme for the integration of the spacetime equations (either ADM or AFA) and Roe's approximate Riemann solver for the hydrodynamical equations. We use "1+log" slicing with $N = 2$.

As in the boson star studies we have first considered evolutions which test separately the individual components of the code. In these, we either solve the hydrodynamical equations in a prescribed (static) spacetime or the gravitational field equations for a prescribed matter source. In particular, we have evolved static neutron star configurations with a zero-temperature polytropic equation of state, of the form $P = K\rho^{\Gamma}$ (where P is pressure and ρ is rest-mass density). This included stars with a large polytropic index Γ (very stiff) having density profiles with a discontinuous first derivative at the surface. In the case of prescribed matter sources, we have confirmed that the comparison of the AFA and AF2 systems to the ADM system, in terms of stability and accuracy, remains the same as in the vacuum cases studied above. Static neutron stars with polytropic index $\Gamma = 2$ have also been studied in [11] using the CT equations with prescribed hydrodynamical sources.

We focus next on the coupled spacetime and hydrodynamical evolution of static Tolman-Oppenheimer-Volkoff (TOV) [48] neutron stars (in isotropic coordinates). Again, we compare the results obtained using the AFA implementation of the CT equations to those of the ADM equations. In principle both the matter distribution inside the star and the spacetime should remain static. In practice they evolve due to truncation errors of the finite-difference scheme, with the hydrodynamics and the spacetime responding to one another. The static TOV solution provides a reference to monitor the accuracy of the coupled numerical evolution. Note that in these evolutions, static outer boundary conditions were used.

In Fig. 13, we show the evolution of the L2-norm of the Hamiltonian constraint for a polytropic, $N = 1$, TOV star of gravitational mass $1.4M_{\odot}$ and compactness ratio $M/R = 0.146$. A 64^3 grid is used to cover the first octant, with $dx = dy = dz = 0.34$km. The dashed line corresponds to the ADM system and the solid line to the AFA system. Again, as in the vacuum studies, we see that the ADM evolution suddenly becomes unstable at roughly 2.7ms, while the AFA evolution remains stable after more than 6ms (we followed the evolution for more than twice that).

In Fig. 14 we show the evolution of the radial component of the metric (constructed from the evolved Carte-

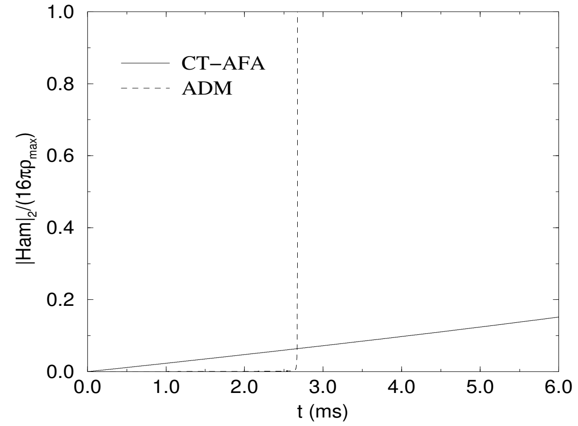

FIG. 13. Evolution of the L2-norm of the Hamiltonian constraint for a N=1.0 polytropic neutron star model (coupled spacetime and hydrodynamical evolution). The ADM system crashes after less than 2.7ms, while the AFA system evolves stably for a significantly longer time. A 64^3-grid was used to cover the first octant.

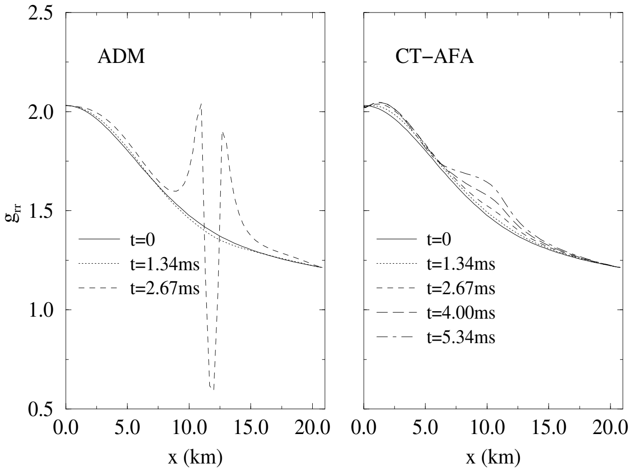

FIG. 14. Comparison of the evolution of the radial metric component for a $N = 1.0$ polytrope with ADM (left panel) and AFA. The evolution with the latter system proceeds well beyond the time at which the ADM system becomes unstable.

sian metric components). The first panel of Fig. 14 corresponds to the evolution obtained with ADM. We see that the star basically maintains its initial equilibrium, until the high-frequency instability crashes the code. In the second panel, we show g_{rr} at various times, obtained with the AFA implementation. All other parameters are the same as in the ADM evolution. The ADM run is more accurate, before it becomes unstable, while the AFA run is stable but less accurate (there is a secular drift away from the initial configuration).

The truncation errors of the coupled evolution code initiate a pulsation of the star in, mainly, its radial modes of pulsation. These pulsations are damped in time due to the viscosity of the numerical scheme (see [49,50]). The TVD schemes we are using describe well the physical pulsations of the fluid, except in a small region around the center of the star, where short wavelength noise appears in the radial velocity. Our trials with other HRSC schemes show that this behavior seems to be generic for higher order HRSC schemes *. In all such schemes, the radial momentum near the center has a small residual value of constant sign. This momentum appears in the r.h.s. of the evolution equation for $\tilde{\Gamma}^i$ (Eq. (20)). This, in turn, leads to an error in the spacetime evolution. It is noteworthy that this does not cause an instability in the coupled evolution, except at very late times, when the violation of the Hamiltonian constraint has already become extremely large.

We note that as the TVD schemes are only first-order accurate at local extrema, such as the maximum of the density at the center of the star, so the increase in the Hamiltonian constraint at the center converges to roughly first order with increasing resolution. Away from the center, the scheme is second order convergent. The convergence of the L2-norm of the Hamiltonian constraint with the AFA system, for different grid-sizes (and for the same initial configuration as above), is shown in Fig. 15.

IV. DISCUSSION AND CONCLUSIONS

In this paper we have studied the stability of three-dimensional numerical evolutions of the Einstein equations in a formulation that separates out the conformal and traceless parts of the system. In our study we have considered different spacetimes including gravitational waves, black holes, boson stars and neutron stars.

We investigated several implementations of the conformal-traceless (CT) evolution equations. We iden-

*We have extensively experimented with other hydrodynamical evolution schemes. If one uses a first-order (Godunov) scheme, using piecewise constant reconstructed data for the Riemann problem, instead of piecewise linear, the radial velocity oscillates around zero near the center of the star, without any short wave length noise. But, a low-order scheme is not capable of accurately describing the evolution of the stellar surface where the density distribution is changing rapidly (unless prohibitively large grids are used) and large errors from the surface layers soon propagate inside the star. We have also experimented with a mixed system: first-order near the center and second-order near the surface. In this case the error grows at the interface of the two regime, yielding a even less accurate evolution overall.

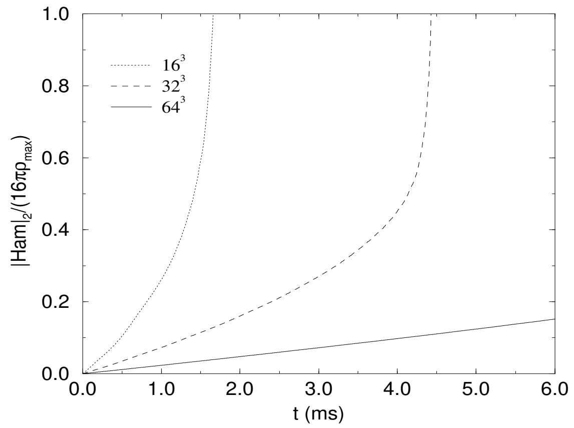

FIG. 15. Convergence of the L2-norm of the Hamiltonian constraint, at three different resolutions, for a N=1.0 polytropic neutron star model. The AFA system is used.

tified two of them which give the best long term stability behavior: the AF2 implementation for maximal slicing, and the AFA for algebraic slicings. The AFA implementation actively enforces the trace of the conformally rescaled extrinsic curvature ($\tilde{A}$) to zero at each step of the time evolution, while the AF2 implementation enforces as well the fact that the trace of the extrinsic curvature (K) should vanish in maximal slicing. On the analytic level, the CT evolution equations imply that $\tilde{A} = 0$ throughout the evolution, but this is inevitably violated in numerically evolution due to truncation error, unless actively enforced. Similarly, for maximal slicing, K will not remain zero numerically unless actively forced to do so. We find that these two implementations of the CT equations lead to a more stable evolution compared to what one can obtain using the standard ADM evolution equations, under the same resolution, boundary condition and grid parameter choices, for all systems investigated. In comparison, a straightforward implementation of the CT equations ("Mom") is capable of giving a stable evolution for weak but not strong field systems. In this paper we focused on the implementations and the numerical properties of their evolutions. Some understanding of the stability of properties is discussed in a companion paper [4].

Beyond stability, we have also compared the accuracy of the evolutions obtained by the ADM equations and CT equations. For all spacetimes considered we have found that the ADM system is consistently more accurate than the CT system in short term evolutions, before the instabilities set in. This points to a direction for possible improvement of the CT approach. We note that formulations combining the CT approach and the hyperbolic approach have been proposed [51,52]. A similar investigation of the stability and accuracy properties of such formulations will be presented elsewhere.

ACKNOWLEDGMENTS

We would like to thank many colleagues for discussions that have aided the development of this work. We are especially grateful to Mark Miller, Malcolm Tobias and Wai-Mo Suen of the Washington University gravity group, to Toni Arbona, Carles Bona, and Joan Massó of the Palma group, to Gabrielle Allen Gerd Lanfermann and Daniel Holz at the AEI, and to Vince Moncrief. The research was supported by AEI, NCSA, the NSF grant Phy 96-00507, NSF NRAC MCS93S025, and NASA HPCC Grand Challenge Grant NCCS5-153. J.A.F. acknowledges financial support from a TMR grant from the European Union (contract nr. ERBFMBICT971902).

APPENDIX A: STABILITY ANALYSIS OF THE ITERATIVE CRANK-NICHOLSON SCHEME

The numerical scheme used for the simulations described in this paper is the so-called iterative Crank-Nicholson (ICN) scheme, which is an iterative, explicit version of the standard implicit Crank-Nicholson (CN) scheme [53,54]. The idea behind this method is to solve the implicit equations by an iterative procedure, where each iteration is an explicit operation depending only on previously computed data. Normally, this process is stopped after a certain number of iterations, or until some tolerance is achieved. For a linear equation (and in particular in one dimension), the iterative procedure can easily be much more computationally expensive than the matrix inversion required to solve the original implicit scheme. For a non-linear system, however, solving the implicit scheme directly can prove to be extremely difficult.

In this appendix we study the stability properties of the ICN scheme in the particular case of the simple wave equation, and derive two very important results:

- In order to obtain a stable scheme one must do *at least* three iterations, and not just the two one would normally expect (two iterations are enough to achieve second order accuracy, but they are unstable!).
- The iterative scheme itself is only convergent if the standard Courant-Friedrichs-Lewy (CFL) stability condition is satisfied, otherwise the iterations diverge.

These two results taken together imply that there is no reason (at least from the point of view of stability) to ever do more that three ICN iterations. Three iterations are already second order accurate, and provide us with a (conditionally) stable scheme. Increasing the number of iterations will not improve the stability properties of the scheme any further. In particular, we will never achieve the unconditional stability properties of the full implicit CN scheme, since if we violate the CFL condition the iterations will diverge. †

For our stability analysis we will consider the simple wave equation in N-dimensions. Numerical experiments have shown that the full Einstein equations have essentially the same stability properties.

Consider then the N-dimensional wave equation written in "3+1 like" form:

$$\partial_t \phi = A, \qquad \partial_t A = \sum_{i=1}^{N} \partial_i^2 \phi. \tag{A1}$$

For the finite difference approximation to these equations we employ the usual notation

$$f^n_{\mathbf{m}} := f(x_i = m_i \Delta x, t = n\Delta t), \tag{A2}$$

with n and $\mathbf{m} = (m_1, ..., m_N)$ integers. The implicit CN scheme is then given by

$$\phi^{n+1}_{\mathbf{m}} = \phi^n_{\mathbf{m}} + \frac{\Delta t}{2}\left(A^{n+1}_{\mathbf{m}} + A^n_{\mathbf{m}}\right), \tag{A3}$$

$$A^{n+1}_{\mathbf{m}} = A^n_{\mathbf{m}} + \frac{\Delta t}{2(\Delta x)^2} \sum_{i=1}^{N} \delta_i^2 \left(\phi^{n+1}_{\mathbf{m}} + \phi^n_{\mathbf{m}}\right), \tag{A4}$$

where the finite difference operators δ_i^2 are defined as

$$\delta_i^2 f^n_{m_i} := f^n_{m_i+1} - 2 f^n_{m_i} + f^n_{m_i-1}. \tag{A5}$$

The implicit CN scheme is well known to be unconditionally stable for the wave equation (i.e. stable for any value of Δt).

The ICN scheme is defined in the following way

$$\phi^{(1)}_{\mathbf{m}} = \phi^n_{\mathbf{m}} + \Delta t \; A^n_{\mathbf{m}}, \tag{A6}$$

$$A^{(1)}_{\mathbf{m}} = A^n_{\mathbf{m}} + \Delta t \sum_{i=1}^{N} \phi^n_{\mathbf{m}}, \tag{A7}$$

$$\phi^{(i)}_{\mathbf{m}} = \phi^n_{\mathbf{m}} + \frac{\Delta t}{2}\left(A^{(i-1)}_{\mathbf{m}} + A^n_{\mathbf{m}}\right), \tag{A8}$$

$$A^{(i)}_{\mathbf{m}} = A^n_{\mathbf{m}} + \frac{\Delta t}{2(\Delta x)^2} \sum_{i=1}^{N} \delta_i^2 \left(\phi^{(i-1)}_{\mathbf{m}} + \phi^n_{\mathbf{m}}\right), \tag{A9}$$

and finally,

$$\phi^{n+1}_{\mathbf{m}} = \phi^{(i_{\max})}_{\mathbf{m}}, \tag{A10}$$

$$A^{n+1}_{\mathbf{m}} = A^{(i_{\max})}_{\mathbf{m}}, \tag{A11}$$

From these expressions it is clear that if the iterations converge, we will recover the implicit CN scheme.

For the stability analysis of the ICN scheme we use the standard von Neumann ansatz [53,56]

$$\phi^n_{\mathbf{m}} = \xi_1 \lambda^n e^{i(\mathbf{k}\cdot\mathbf{m})\Delta x}, \tag{A12}$$

$$A^n_{\mathbf{m}} = \xi_2 \lambda^n e^{i(\mathbf{k}\cdot\mathbf{m})\Delta x}, \tag{A13}$$

with $\mathbf{k}$ the "wave vector". Notice that the highest wave number that can be represented on the finite difference grid corresponds to $k_i \Delta x = \pi$. The stability condition for our numerical scheme will then be

$$|\lambda| \leq 1. \tag{A14}$$

Let us consider first the "1-step" ICN scheme, that is, the so-called forward-time centered-space (FTCS) scheme. This scheme is well known to be only first order accurate, and unconditionally unstable. The fact that is only first order accurate can be easily seen from a simple Taylor expansion in time. For the stability analysis we substitute the von Neumann ansatz (A13) into the ICN scheme defined above with $i_{\max} = 1$. Doing this we obtain

$$\lambda^2 - 2\lambda + 1 + 2\rho^2 u^2 = 0, \tag{A15}$$

where $\rho := \Delta t / \Delta x$ is the Courant parameter and

$$u^2 := \sum_{i=1}^{N} u_i^2, \tag{A16}$$

$$u_i^2 := 1 - \cos(k_i \Delta x). \tag{A17}$$

Solving for λ we find

$$\lambda = 1 \pm i\sqrt{2}\,\rho u, \tag{A18}$$

which implies

$$|\lambda| = 1 + 2\rho^2 u^2 > 1. \tag{A19}$$

Comparing with (A14) we conclude that the 1-step scheme is unstable for any value of Δt.

Let us now consider the 2-step scheme. If we take the ICN scheme above with $i_{\max} = 2$, and do the appropriate substitutions we find

$$\phi^{n+1}_{\mathbf{m}} = \phi^n_{\mathbf{m}} + \Delta t \; A^n_{\mathbf{m}} + \frac{\rho^2}{2} \sum_{i=1}^{N} \delta_i^2 \; \phi^n_{\mathbf{m}}, \tag{A20}$$

$$A^{n+1}_{\mathbf{m}} = A^n_{\mathbf{m}} + \frac{\rho^2}{2} \sum_{i=1}^{N} \delta_i^2 \; \left(2\phi^n_{\mathbf{m}} + \Delta t A^n_{\mathbf{m}}\right). \tag{A21}$$

As before, a simple Taylor expansion shows that this approximation is now second order both in time and space.

† As we were finishing this manuscript we became aware of a paper by S. Teukolsky were he does essentially the same analysis and obtains the same results [55]. His analysis and ours complement each other, since he considers any finite number of iterations, while we consider only 1, 2 and 3 iterations. On the other hand, here we also consider the question of the convergence properties of an *infinite* number of iterations.

Using again the ansatz (A13) we find now that

$$\lambda^2 + 2\lambda\left(\rho^2 u^2 - 1\right) + 1 + \rho^4 u^4 = 0. \tag{A22}$$

Solving again for λ we obtain

$$\lambda = 1 - \rho^2 u^2 \pm i\sqrt{2}\,\rho u, \tag{A23}$$

which implies

$$|\lambda| = 1 + \rho^4 u^4 > 1. \tag{A24}$$

Comparing again with (A14) we conclude that the 2-step ICN scheme is also unstable for any value of Δt. This result is surprising, since a priori one might expect that the 2-step scheme should behave like a predictor-corrector scheme, and should therefore be stable.

Finally, let us consider the 3-step scheme. By taking the ICN scheme above with $i_{\max} = 3$, and doing the appropriate substitutions we now find

$$\phi^{n+1}_{\mathbf{m}} = \phi^n_{\mathbf{m}} + \Delta t A^n_{\mathbf{m}} + \frac{\rho^2}{4}\sum_{i=1}^{N}\delta_i^2\left(2\phi^n_{\mathbf{m}} + \Delta t A^n_{\mathbf{m}}\right), \tag{A25}$$

$$A^{n+1}_{\mathbf{m}} = A^n_{\mathbf{m}} + \frac{\rho^2}{2}\sum_{i=1}^{N}\delta_i^2\,\left(2\phi^n_{\mathbf{m}} + \Delta t A^n_{\mathbf{m}}\right) + \frac{\rho^3}{4\Delta x}\left(\sum_{i=1}^{N}\delta_i^2\right)^2\phi^n_{\mathbf{m}}. \tag{A26}$$

A Taylor expansion now shows that this 3-step scheme is still only second order accurate in both time and space. Using the ansatz (A13) on this scheme we now find

$$\lambda^2 + 2\lambda\left(\rho^2 u^2 - 1\right) + 1 - \rho^4 u^4 + \frac{1}{2}\rho^6 u^6 = 0. \tag{A27}$$

And solving for λ we obtain

$$\lambda = 1 - \rho^2 u^2 \pm i\sqrt{2}\,\rho u\left|1 - \rho^2 u^2/2\right|, \tag{A28}$$

which now implies

$$|\lambda| = 1 - \rho^4 u^4 + \frac{1}{2}\rho^6 u^6. \tag{A29}$$

Comparing now with (A14) we obtain the following stability condition

$$\rho^2 u^2 \leq 2. \tag{A30}$$

And finally, from the fact that the maximum value of u^2 is $2\sqrt{N}$ we find

$$\rho \leq 1/\sqrt{N}. \tag{A31}$$

Notice that this is just the standard CFL condition in N dimensions. We then conclude that in order to obtain a (conditionally) stable scheme we need to do at least three iterations.

Next, we address the question of the stability of the iterations themselves, that is, if we iterate an infinite number of times do we converge to something (that is, to the implicit CN scheme)? For this we consider two consecutive iteration steps $(i-1, i)$, and subtract them to get

$$\phi^{(i)}_{\mathbf{m}} - \phi^{(i-1)}_{\mathbf{m}} = \frac{\Delta t}{2}\left(A^{(i-1)}_{\mathbf{m}} - A^{(i-2)}_{\mathbf{m}}\right), \tag{A32}$$

$$A^{(i)}_{\mathbf{m}} - A^{(i-1)}_{\mathbf{m}} = \frac{\Delta t}{2(\Delta x)^2}\sum_{i=1}^{N}\left(\phi^{(i-1)}_{\mathbf{m}} - \phi^{(i-2)}_{\mathbf{m}}\right). \tag{A33}$$

Let us now define $F1^{(i)}_{\mathbf{m}} := \phi^{(i)}_{\mathbf{m}} - \phi^{(i-1)}_{\mathbf{m}}$ and $F2^{(i)}_{\mathbf{m}} := A^{(i)}_{\mathbf{m}} - A^{(i-1)}_{\mathbf{m}}$. The above equations become

$$F1^{(i)}_{\mathbf{m}} = \frac{\Delta t}{2}F2^{(i-1)}_{\mathbf{m}}, \tag{A34}$$

$$F2^{(i)}_{\mathbf{m}} = \frac{\Delta t}{2(\Delta x)^2}\sum_{i=1}^{N}F1^{(i-1)}_{\mathbf{m}}. \tag{A35}$$

We now use the von Neumann ansatz again

$$F1^{(i)}_{\mathbf{m}} = f_1\lambda^i e^{i(\mathbf{k}\cdot\mathbf{m})\Delta x}, \tag{A36}$$

$$F2^{(i)}_{\mathbf{m}} = f_2\lambda^i e^{i(\mathbf{k}\cdot\mathbf{m})\Delta x}, \tag{A37}$$

Substituting this ansatz back into the equations above we find

$$\lambda^2 + \frac{1}{2}\rho^2 u^2 = 0, \tag{A38}$$

from which we obtain

$$\lambda = \pm i\frac{\rho u}{\sqrt{2}}. \tag{A39}$$

In this case, the condition for the iterations to converge implies that the norm of the successive differences should go to zero, which in turn implies $|\lambda| < 1$. Using again the fact that the maximum value of u^2 is $2\sqrt{N}$ we see that the convergence condition reduces to

$$\rho < 1/\sqrt{N}. \tag{A40}$$

This is again the standard CFL stability condition. So we have just shown that if this condition is violated, the iterations will fail to converge. This means that there is no reason to try to iterate to convergence in the hope of improving stability. If Δt was too big in the first place the iterations will never converge.

[1] Éanna É. Flanagan and S. A. Hughes, Phys. Rev. D **57**, 4535 (1998), gr-qc/9701039.

[2] Éanna É. Flanagan and S. A. Hughes, Phys. Rev. D **57**, 4566 (1998), gr-qc/9710129.
[3] R. Arnowitt, S. Deser, and C. W. Misner, in *Gravitation: An Introduction to Current Research*, edited by L. Witten (John Wiley, New York, 1962), pp. 227–265.
[4] M. Alcubierre, G. Allen, B. Brügmann, E. Seidel, and W.-M. Suen, (1999), gr-qc/9908079.
[5] T. Nakamura, K. Oohara, and Y. Kojima, Prog. Theor. Phys. Suppl. **90**, 1 (1987).
[6] T. Nakamura and K. Oohara, in *Frontiers in Numerical Relativity*, edited by C. Evans, L. Finn, and D. Hobill (Cambridge University Press, Cambridge, England, 1989), pp. 254–280.
[7] M. Shibata and T. Nakamura, Phys. Rev. D **52**, 5428 (1995).
[8] T. Nakamura and K. ichi Oohara, (1999), gr-qc/9812054.
[9] M. Shibata, Prog. Theor. Phys. **101**, 1199 (1999), gr-qc/9905058.
[10] T. W. Baumgarte and S. L. Shapiro, Physical Review D **59**, 024007 (1999).
[11] T. W. Baumgarte, S. A. Hughes, and S. L. Shapiro, (1999), gr-qc/9902024.
[12] M. Shibata, Phys. Rev. D **60**, 104052 (1999), gr-qc/9908027.
[13] M. Shibata and K. Uryu, Phys. Rev. D **61**, 064001 (2000), gr-qc/9911058.
[14] M. Shibata, T. W. Baumgarte, and S. L. Shapiro, Phys. Rev. D , in press; gr-qc/9911308.
[15] J. York, in *Sources of Gravitational Radiation*, edited by L. Smarr (Cambridge University Press, Cambridge, England, 1979).
[16] H. Friedrich, private communication.
[17] A. Arbona, C. Bona, J. Massó, and J. Stela, gr-qc/9902053 (1999).
[18] C. Bona, J. Massó, E. Seidel, and J. Stela, Phys. Rev. Lett. **75**, 600 (1995).
[19] D. Bernstein, Ph.D. thesis, University of Illinois Urbana-Champaign, 1993.
[20] M. Alcubierre, Phys. Rev. D **55**, 5981 (1997).
[21] M. Alcubierre and J. Massó, Phys. Rev. D Rapid Comm. **57**, 4511 (1998).
[22] B. Gustafsson and H. Kreiss, J. Comp. Phys. **30**, 333 (1979).
[23] P. Anninos, J. Massó, E. Seidel, W.-M. Suen, and M. Tobias, Phys. Rev. D **56**, 842 (1997).
[24] M. Alcubierre, G. Allen, B. Brügmann, G. Lanfermann, E. Seidel, W.-M. Suen, and M. Tobias, (1999), gr-qc/9904013.
[25] D. S. Brill, Ann. Phys. **7**, 466 (1959).
[26] D. Holz, W. Miller, M. Wakano, and J. Wheeler, in *Directions in General Relativity: Proceedings of the 1993 International Symposium, Maryland; Papers in honor of Dieter Brill*, edited by B. Hu and T. Jacobson (Cambridge University Press, Cambridge, England, 1993).
[27] K. Eppley, in *Sources of Gravitational Radiation*, edited by L. Smarr (Cambridge University Press, Cambridge, England, 1979), p. 275.
[28] M. Shibata, Phys. Rev. D **55**, 7529 (1997).
[29] A. Gentle, D. Holz, W. Miller, and J. Wheeler, Class. Quant. Grav. **16**, 1979 (1999), gr-qc/9812057.
[30] K. Camarda, Ph.D. thesis, University of Illinois at Urbana-Champaign, Urbana, Illinois, 1998.
[31] G. Allen, K. Camarda, and E. Seidel, (1998), gr-qc/9806036, submitted to Phys. Rev. D.
[32] S. Brandt, K. Camarda, and E. Seidel, in preparation (unpublished).
[33] S. Brandt, K. Camarda, and E. Seidel, in *Proc. 8th M. Grossmann Meeting*, edited by T. Piran (World Scientific, Singapore, 1998), in press.
[34] J. Balakrishna, G. Daues, E. Seidel, W.-M. Suen, M. Tobias, and E. Wang, Class. Quant. Grav. **13**, L135 (1996).
[35] P. Anninos, K. Camarda, J. Massó, E. Seidel, W.-M. Suen, and J. Towns, Phys. Rev. D **52**, 2059 (1995).
[36] P. Anninos, J. Massó, E. Seidel, and W.-M. Suen, Physics World **9**, 43 (1996).
[37] B. Brügmann, Int. J. Mod. Phys. D **8**, 85 (1999).
[38] J. Thornburg, Classical and Quantum Gravity **4**, 1119 (1987).
[39] E. Seidel and W.-M. Suen, Phys. Rev. Lett. **69**, 1845 (1992).
[40] R. Gomez *et al.*, Phys. Rev. Lett. **80**, 3915 (1998), gr-qc/9801069.
[41] J. A. Font, M. Miller, W. M. Suen, and M. Tobias, Phys. Rev. D **61**, 044011 (2000).
[42] E. Seidel and W.-M. Suen, Phys. Rev. D **42**, 384 (1990).
[43] J. Balakrishna and H. Shinkai, Physical Review D **58**, 044016 (1998).
[44] J. Balakrishna, E. Seidel, and W.-M. Suen, Physical Review D **58**, 104004 (1998), gr-qc/9712064.
[45] M. Choptuik, Phys. Rev. Lett. **70**, 9 (1993).
[46] T. Dramlitsch, Master's thesis, Universität Potsdam, 1999.
[47] J. Balakrishna, Ph.D. thesis, Wahington University, St. Louis, 1999.
[48] C. W. Misner, K. S. Thorne, and J. A. Wheeler, *Gravitation* (W. H. Freeman, San Francisco, 1973).
[49] N. Stergioulas, J. A. Font, and K. Kokkotas, (1999), gr-qc/9904009.
[50] J. A. Font, N. Stergioulas, and K. D. Kokkotas, (2000), mNRAS in press, gr-qc/9908010.
[51] M. Alcubierre, B. Brügmann, M. Miller, and W.-M. Suen, Phys. Rev. **D60**, 064017 (1999), gr-qc/9903030.
[52] S. Frittelli and O. Reula, (1999).
[53] B. Gustafsson, H.-O. Kreiss, and J. Oliger, *Time dependent problems and difference methods* (Wiley, New York, 1995).
[54] K. C. B. New, K. Watt, C. W. Misner, and J. M. Centrella, Phys. Rev. D **58**, 064022 (1998), gr-qc/9801110.
[55] S. Teukolsky, (1999), gr-qc/9909026.
[56] W. H. Press, B. P. Flannery, S. A. Teukolsky, and W. T. Vetterling, *Numerical Recipes* (Cambridge University Press, Cambridge, England, 1986).